JOURNAL OF MATERIALS SCIENCE 17 (1982) 2567–2576

Compression fatigue behaviour of notched composite laminates

R. M. WALSH Jr, R. B. PIPES
Center for Composite Materials, University of Delaware, Newark, Delaware 19711, USA

The influence of compression fatigue on graphite/epoxy laminates containing circular holes of 0.635 cm diameter was investigated. The laminate stacking sequences were $[0_2°/\pm 45°]_{5s}$, $[0°/45°/0/-45°]_{5s}$, $[0°/\pm 45°/90°]_{5s}$ and $[90°/0°/\pm 45°]_{5s}$. Specifically this study examined the nature and extent of induced compression fatigue damage and determined the effects of this damage on the laminate residual failure mechanisms. Two modes of compression failure were found to occur: diagonal shear and net compression. Both failure modes were characterized by local instability of individual lamina or small lamina subgroupings, with diagonal shear predominant in the fibre-dominated laminates and net compression predominant in the quasi-isotropic laminates. The mode and direction of failure were dependent upon the nature of the specimen delamination. It was also found that the laminate stacking sequence influenced the intraply crack development in the laminates as well as the failure mode. The failure mechanisms were essentially the same for the two different material systems which were studied (Narmco 5208 and 5209).

1. Introduction

The increasing use of graphite/epoxy laminates in the aerospace industry, along with the potential for more widespread structural applications in the future, places a significant emphasis on understanding the fatigue characteristics of these materials. Such understanding is essential in facilitating the efficient and safe design of structures utilizing these laminates. Fatigue studies dealing with tension–tension cycling have resulted in favourable behaviour which is superior to that of metals [1, 2]. Other studies of composites in tension–compression and compression–compression fatigue [2], however, indicate a substantial reduction in the fatigue life as compared to the tension–tension case. This behaviour underscores the added importance of fully characterizing the fatigue behaviour and failure mechanisms resulting from compressive loading.

The mechanism of failure in compressive fatigue [1] has been observed as beginning with local matrix failure in the vicinity of a stress concentration. Failure of the matrix then leads to fibre splitting followed by progressive delamination and local instability. In view of this deleterious mechanism of failure, an area of particular interest is that of compression–compression fatigue of notched laminates. It is this topic which was the subject of this work.

This experimental study focused on the characterization of the nature and extent of the induced fatigue damage in the graphite/epoxy laminate, specifically in the vicinity of a circular hole. Of particular interest are the mechanisms of failure corresponding to compressive residual strength tests. Specimens of each laminate were tested statically to establish the initial static strength, and identical specimens were then subjected to compression–compression fatigue loading to induce damage in the area of a circular hole. Throughout the programme, nondestructive evaluation (NDE) of the damage was performed by means of ultrasonic C-scan techniques. Test samples were also dissected for micrographic analysis. The failure mechanisms of the fatigued specimens were observed by means of subsequent static compressive loading to failure.

2. Test programme

Fabrication of the test specimens was performed

0022–2461/82/092567–10$03.70/0

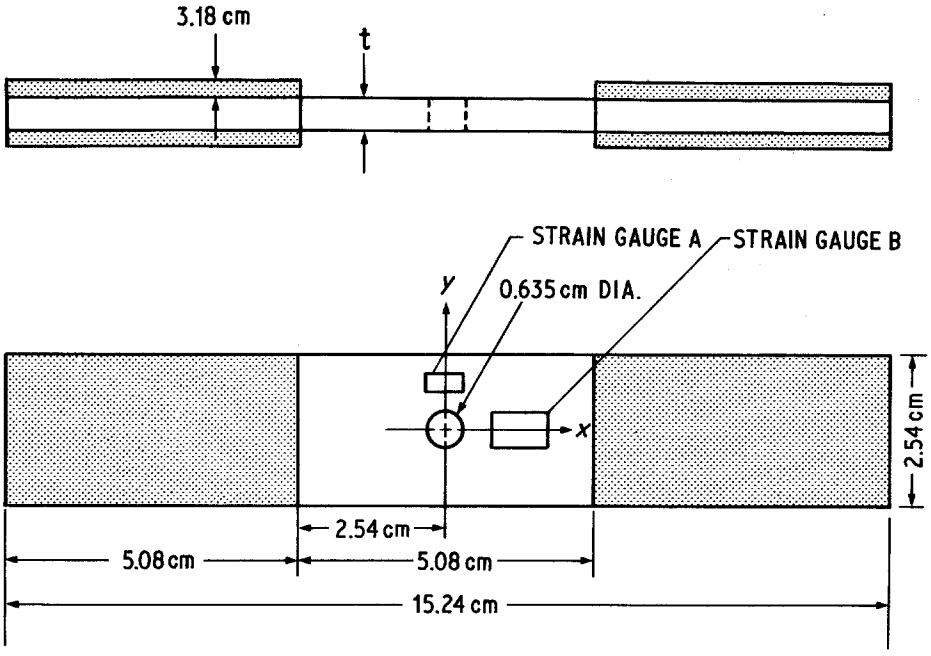

Figure 1 Notched fatigue specimen.

using Narmco (T300/5208 and T300/5209) graphite/epoxy prepreg material. Four laminate configurations were examined for each resin system and are denoted as Laminates A, B, C and D as follows:

A: $[0/0/45/-45/0/0/45/-45/0/0/45/-45/0/0/45/-45/0/0/45/-45]_s$,

B: $[0/45/0/-45/0/45/0/-45/0/45/0/-45/0/45/0/-45/0/45/0/-45]_s$,

C: $[0/45/-45/90/0/45/-45/90/0/45/-45/90/0/45/-45/90/0/45/-45/90]_s$,

and

D: $[90/0/45/-45/90/0/45/-45/90/0/45/-45/90/0/45/-45/90/0/45/-45]_s$.

Panels with these stacking sequences were laid up and cured in an autoclave using a two-step cure cycle with maximum process temperatures of 117° C for 5208 and 121° C for 5209, and a pressure of 0.586 to 0.689 MPa with no post-curing. The endtab material was a glass-reinforced, epoxy resin material. The adhesive used to bond the entabs to the graphite/epoxy specimens was Hysol Aerospace Adhesive EA 9309 which was selected because of its high peel strength.

The test specimen configuration and dimensions are shown in Fig. 1. The specimens were 2.54 cm in width with a 0.635 cm diameter circular hole centrally located in the unsupported span. In determining the length of the unsupported span (gauge length), the objective was to maximize this dimension, and thereby minimize any grip effects, without reaching a state of instability which would result in gross buckling of the laminate. A gauge length of 5.08 cm was selected and found to exhibit no signs of gross laminate buckling based on strain gauge readings made of selected specimens in static tests. All tests were performed with an Instron Model 1321 closed-loop, servo-hydraulic test machine. The test fixture was the modified IITRI* compression fixture shown in Fig. 2 [3].

Specimens of each laminate were tested statically to establish the initial static strength. Other identical specimens were subjected to fatigue loading followed by residual strength evaluation. The fatigue schedule is summarized in Table I. Certain of the test samples were sectioned after fatigue loading in order to conduct micrographic analyses. The section orientations are shown in Fig. 3.

Progressive damage characterization of specimens subjected to fatigue loading was monitored through the use of ultrasonic C-scan techniques

*Illinois Institute of Technology Research Institute.

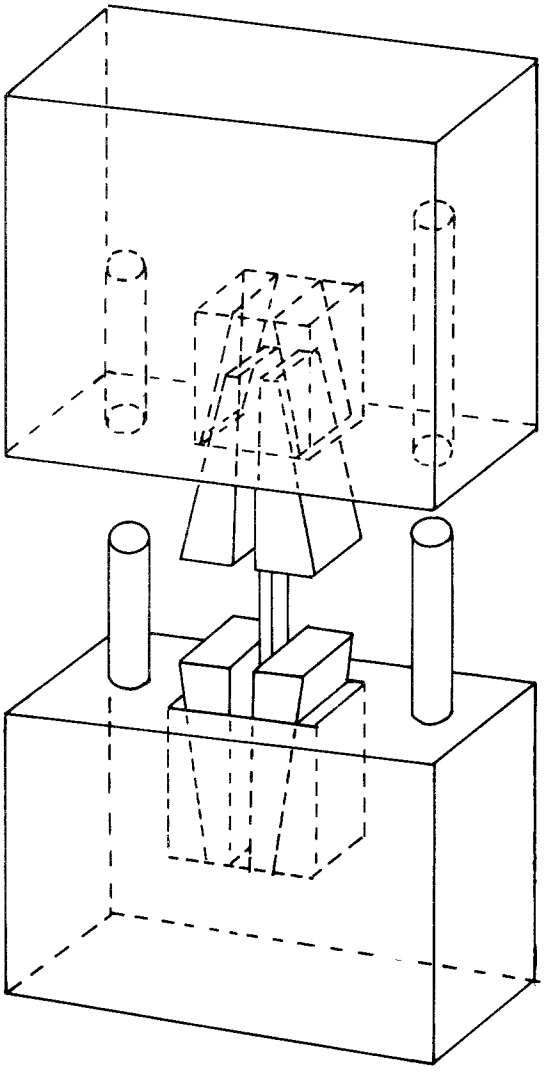

Figure 2 Modified IITRI compression fixture.

TABLE I Fatigue programme ($R = 0.1$; frequency of 10 Hz; ambient conditions)

Specimen	S-level	Cycles
1	(Static)	–
2	(Static)	–
3	(Static)	–
4	0.50	1×10^6
5	0.50	1×10^6
6	0.50	1×10^6
7	0.60	1×10^6
8	0.60	1×10^6
9	0.60	1×10^6
10	0.60	5×10^5
11	0.60	5×10^5
12	0.60	5×10^5

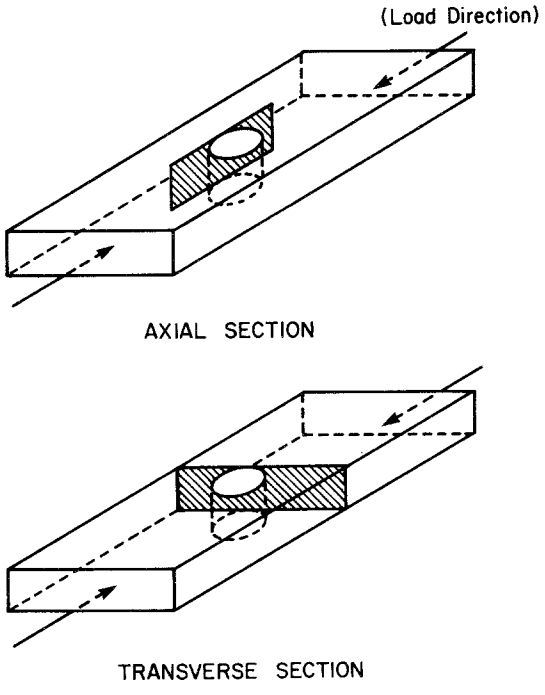

Figure 3 Micrograph section orientations.

which were utilized as a means of nondestructive evaluation (NDE). The specific technique employed was the peak amplitude based C-span [4]. In order to monitor the initiation and subsequent growth of the fatigue-induced damage, all specimens were removed from the test machine at regular intervals of 2.5×10^5 cycles and inspected via the C-scan. Upon completion of the fatigue tests, a series of C-scans was assembled from which the damage sequence could be characterized.

3. Failure mechanisms

Since the two resin systems (5208 and 5209) possessed different maximum process temperatures, it was expected that resin-controlled failure mechanisms might be different for the two systems. In actuality, the static failure mechanisms for the two material systems were indistinguishable. However, the failure mechanisms for the four laminates exhibited significant differences. Two distinct failure modes were observed for Laminate A. They were the diagonal shear (DS) failure mode and the net compression (NC) failure mode, which are illustrated in Fig. 4.

Fatigue damage in Laminate A was manifest as cracking of the $+45°$ and $-45°$ laminae in regions adjacent to the central notch. In regions where the $+45°$ laminae were cracked, the $-45°$ laminae

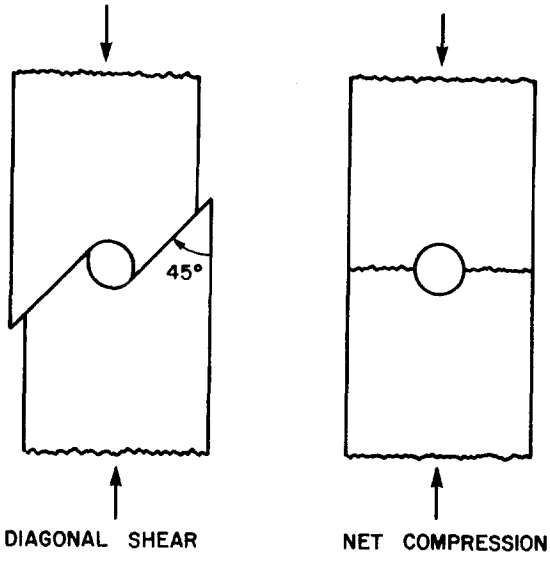

Figure 4 Notched compression failure modes.

were not, and in the regions where the $-45°$ laminae were cracked, the $+45°$ laminae were not, as illustrated in Figs 5 and 6. As can be seen, the $-45°$ laminae exhibited cracking in the first and third quadrants while the $+45°$ laminae cracked in the second and fourth quadrants.

The origin of the fatigue crackings in the $\pm 45°$ laminae must be attributed to the shearing stresses which act at a tangent to the circular notch and parallel to the load direction. The distribution of the shearing stress in this region is an antisymmetric function, as shown in Fig. 7. The direction of the shearing stress may be determined by a free-body diagram as in Fig. 8. Acting at the remote end of the free body is the constant, applied stress $\bar{\sigma}$, while at the section adjacent to the hole, the compressive stress varies from $K_T^{\infty}\bar{\sigma}$ * at the edge of the hole to $\bar{\sigma}$ at some distance from the hole. Since the two resultant forces are not equal, a third force is required for equilibrium. The third force is the resultant of the shearing stress and its direction is the same as the remote applied stress since the resultant force at the section adjacent to the hole will always be greater than the resultant of the remote stress. Hence, when the shearing stress is transformed to a co-ordinate system rotated 45° from the axis of the specimen, transverse tensile stresses act on the $-45°$ laminae and transverse compressive stresses act on the $+45°$ laminae in the first and third quadrants. This behaviour is reversed in the second and fourth quadrants, as shown in Fig. 9.

One significant observation of the residual strength failure of Laminate A was that the diagonal shear failure appeared to be primarily responsible for laminate failure, although net compression failure mode was also present. Further, the diagonal shear failure mode always occurred parallel to the $+45°$ laminae. No $-45°$ diagonal shear failures were observed for Laminate A. Since the $+45°$ laminae in Laminate A are located nearest the surface, it might be expected that cracks in these laminae, developed during fatigue

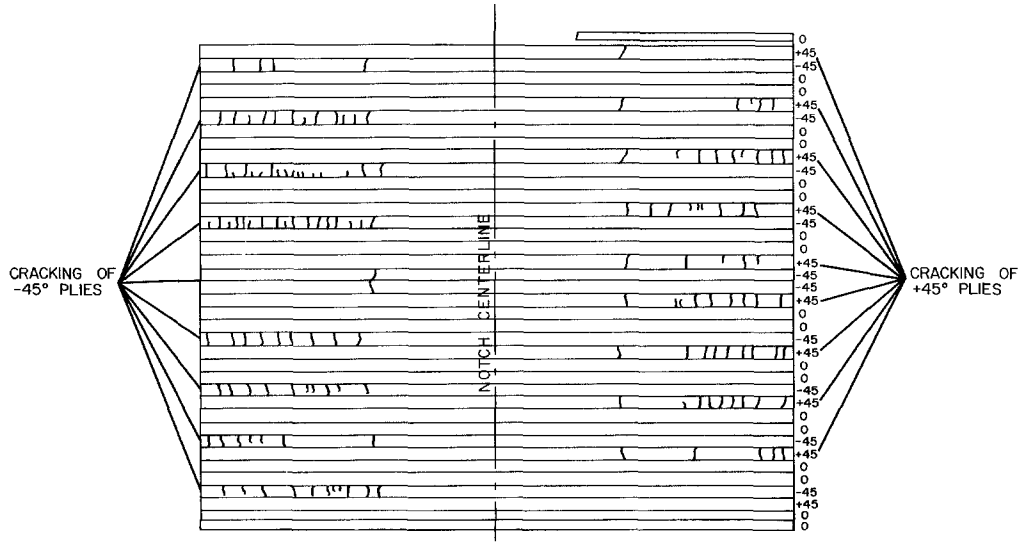

Figure 5 Laminate A $[O_2°/\pm 45°]_{5S}$ axial section (X 50).

* Where K_T^{∞} is the elastic stress concentration factor.

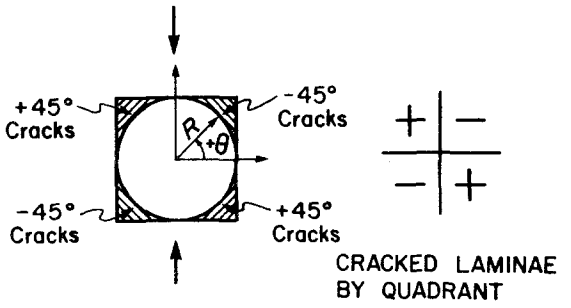

Figure 6 Fatigue crack pattern.

cycling, may play a role in the ultimate failure mode.

Another mechanism characteristic of Laminate A was fatigue growth of cracks in the 0° laminae parallel to the load direction and at a tangent to the edge of the circular notch. The cracks occurred in all 0° laminae only, with their surfaces contained in a single plane at a tangent to the notch as shown in Fig. 10. The delamination which grew at the intersections of the axial cracks and the near-surface 0°/45° interface were mapped in planform by ultrasonic techniques. As can be seen in Fig. 11, the delamination progresses monotonically with increasing cycles or stress amplitude.

The delamination progression was such that it initiated on both sides of the notch at the axial tangent points and propagated towards the end-tabs, as shown in Fig. 11. The regions of delamination initially developed in four quadrants about the notch in a uniform and symmetric manner. Growth of each region progressed along the axial tangent line to the notch, as well as along the circumference of the notch towards the centre of the specimen. The circumferential progression eventually resulted in the bridging of the delamination in the upper two quadrants and, similarly, the lower two quadrants. Upon completion of the joining of these regions, the delamination continued towards the endtabs, contained within a region bounded by the axial tangent lines to the notch.

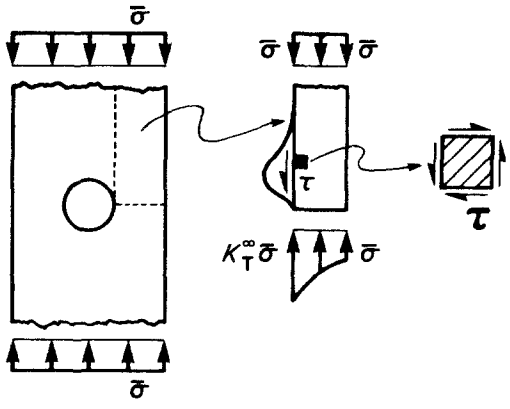

Figure 8 Direction of the shearing stress, τ.

Laminate B failures were similar to those of Laminate A in that they also exhibited characteristics of the diagonal shear and the net compression failure modes. Diagonal shear was the predominant mode of failure with net compression appearing in a small number of instances. In contrast to Laminate A, the shearing direction was not always parallel to the near-surface angle ply (+45°). The failures occurred in the −45°

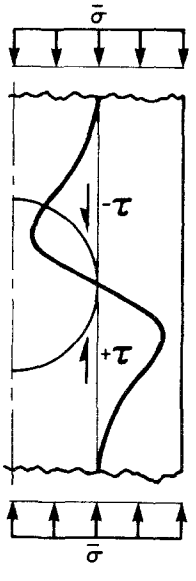

Figure 7 Antisymmetric distribution of the shearing stress, τ.

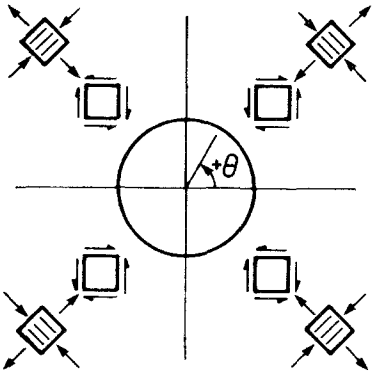

Figure 9 Shear-induced transverse tensile stresses.

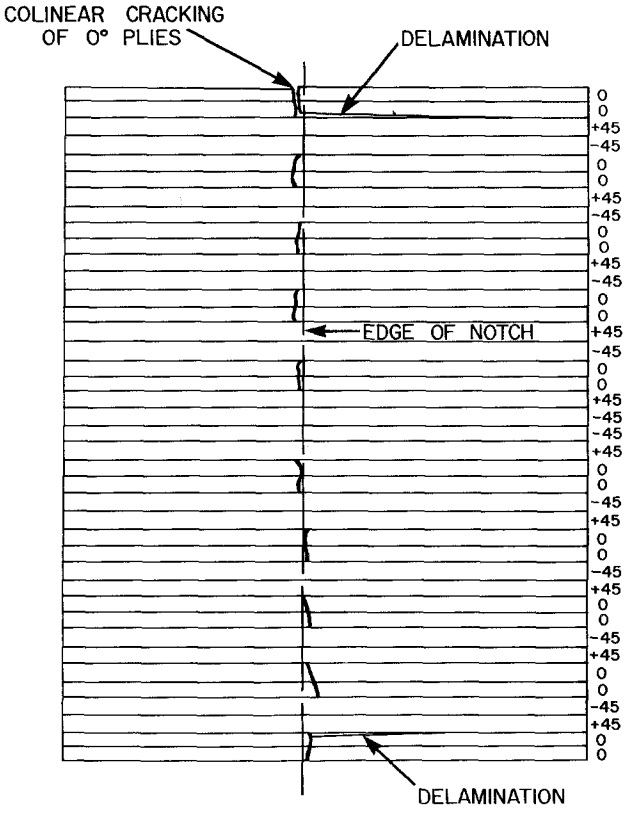

Figure 10 Laminate A $[0_2^\circ/\pm 45^\circ]_{5S}$ transverse section (X 50).

direction as well as the $+45^\circ$ direction. Another distinct shear failure which was observed was the "dual shear" failure in which the shear failure was in the $+45^\circ$ direction on one side of the notch, and in the -45° direction on the other side of the notch, as illustrated in Fig. 12. In characterizing each of these shear failures, it was found that the mode of delamination determined the direction of failure. In all instances, the specimen delamination was such that subgroups of two 0° plies with an angle ply "sandwiched" in between were formed. This resulted in two types of delamination which determined the diagonal shear failure direction. The first case (I) is that in which the subgroups had a configuration of $[0/+45/0]$. In this case, the direction of shear failure was that of the $+45^\circ$ lamina. The subgroups of the second case (II) had a $[0/-45/0]$ configuration resulting in a -45° shear direction. Dual shear failure took place when both delamination cases were present, with Case I on one side of the notch and Case II on the other side. A similar effect was present in Laminate A in which the $0/+45$ interface consistently remained intact, resulting in a $+45^\circ$ shear direction.

A further observation pertaining to the diagonal

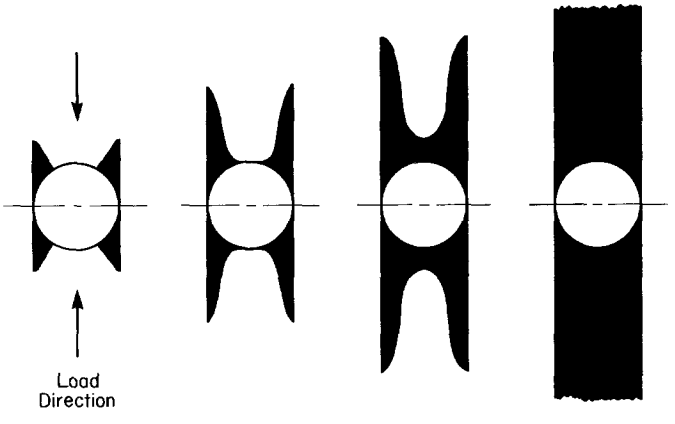

Figure 11 Near-surface delamination growth: Laminate A.

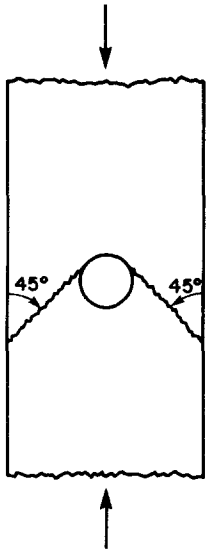

Figure 12 Dual shear compression failure mode.

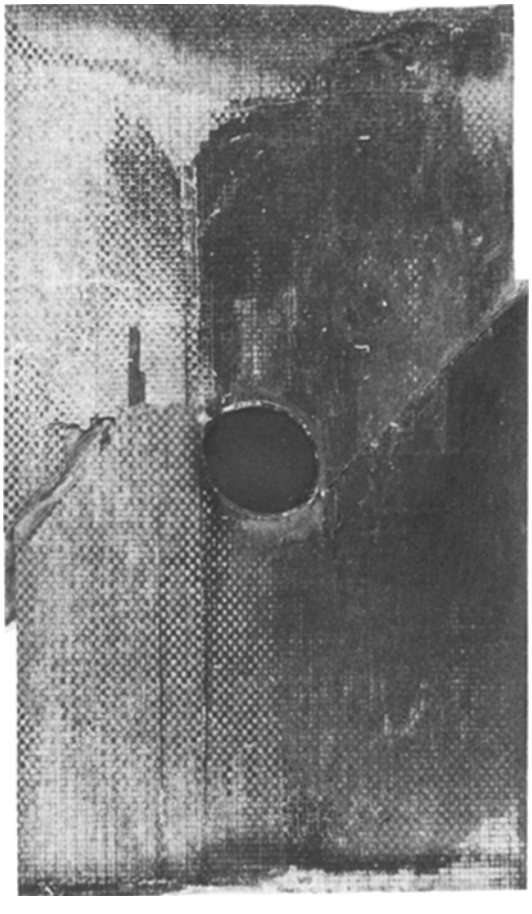

Figure 13 Laminate B diagonal shear failure.

shear failure mode was that the origin of the crack appeared to be at the 45° tangent point to the hole, as shown in Fig. 13. Also, microscopic analysis of Laminate B revealed that while intralaminar cracking of the angle plies was present as in Laminate A, it occurred to a lesser degree. This result is apparently linked to the difference in stacking sequence between Laminates A and B. Despite this, however, the cracking of the angle plies and its subsequent relation to the diagonal shear failure mode observed in Laminate B is consistent with the previous explanation of this failure mode in Laminate A.

The net compression failure mode was present with the diagonal shear failure mode in only a small number of specimens tested. In those instances, it was generally confined to the near-surface layers with the shear failure extending through most of the specimen thickness. The net compression failures were characterized by delamination between the angle plies and the 0° plies, leaving individual 0° plies unsupported and prone to local instability. This is in contrast to the subgroupings of the 0° plies and the angle plies in the diagonal shear mode. Between the zones of diagonal shear and net compression, failures were large interlaminar cracks which extended past the damage zone parallel to the loading direction, as well as from edge to edge in the transverse direction.

The overall failure sequence in Laminate B was one dominated by the angle plies, as has been shown. In this sequence, out-of-plane deformation causes delamination of the laminate into subgroups and induces bending stresses which fail the 0° plies parallel to the cracks in the "sandwiched" angle ply, the direction being determined by that of the angle ply. Net compression infrequently followed the shear failure due to asymmetric loading, which resulted after the shear failure had ceased at the previously mentioned large interlaminar crack.

The mode of near-surface delamination in Laminate B proved to be the same as that described for Laminate A, the significant contrasting element being the degree with which the delamination took place. Specifically, the delamination monitored in Laminate B did not develop to the extent that it did in Laminate A despite comparable stress levels and number of fatigue cycles. Delamination in Laminate B was generally confined to small regions in the four quadrants, often with no significant delamination in a number of the quadrants.

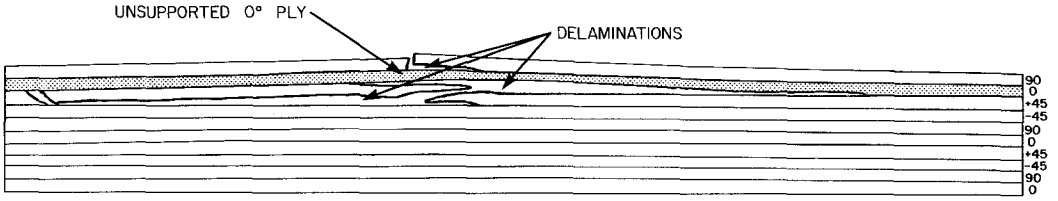

Figure 14 Laminate D $[90°/0°/\pm 45°]_{5S}$ axial section (× 50).

The quasi-isotropic laminates C and D exhibited failure mechanisms common to both. The predominant failure mode was that of net compression with the fracture line running transversely to the loading direction, and directly through the centre of the notch. Extensive interlaminar cracks were observed extending past the damage zone parallel to the loading direction and from edge to edge in the transverse direction. These were similar to those observed in laminates A and B which were present between zones of diagonal shear and net compression failure. In most, cases, the cracks developed at the 0°/+45° interface.

Microscopic inspection of Laminates C and D revealed minimal intralaminar cracking of the individual laminae, particularly the angle plies, which contrasts with the results found in Laminate A. An explanation for this may be made based on the presence of both 0° and 90° plies in the quasi-isotropic laminates which effectively resist both components of shear stress by strengthening the laminate in both the axial and transverse directions. Their presence results in a reduction of the transverse deformation of the angle plies and, hence, a reduction in the cracking as well.

Also discovered in the microscopic inspection was the presence of fatigue-induced delamination at the 0°/+45° interface initiating in the near-surface layers. An additional factor to be considered in the failure of the quasi-isotropic laminates is that the presence of a 90° ply in the stacking sequence results in a reduced axial stiffness in the quasi-isotropic laminate. Such a decrease leads to an increased tendency for local and global instability.

The various factors observed in the failure of the quasi-isotropic laminates indicate that failure is the result of local instability of the individual 0° plies. This is supported by the previous findings which reveal a failure sequence involving delamination of the 0° plies and their adjacent, uncracked 45° plies, leaving unsupported individual 0° plies which subsequently fail in a Mode I buckling failure. Such a sequence initiates in the outermost plies and progresses towards the centre of the laminate. An example of such a configuration is shown in Fig. 14.

The fatigue-induced delamination in the near-surface layers of Laminate C developed in essentially the same manner as that described for Laminate A occurring also at the 0°/+45° interface nearest the surface. The one difference which was found was that in Laminate C the regions of delamination did not remain confined within the two axial tangent lines to the notch as was the case in Laminate A. The delamination was observed to extend in the transverse direction beyond these lines, thereby encompassing the entire perimeter of the notch, as in Fig. 15. This transverse development was relatively small, however, with the primary direction of delamination progression being the axial one, as in Laminates A and B.

The near-surface delamination found in Laminate D was interesting in that while it also initially formed in the four quadrants as described for Laminate A, the primary direction of delamination progression was the transverse direction. The regions of delamination were not confined within the transverse tangent lines to the notch, but instead extended in the axial direction, encompassing the notch perimeter as in Laminate C. This near-surface delamination took place at the outmost 90°/0° interface and is illustrated in Fig. 16.

Based on these results, and those of the ultrasonic examinations of the other three laminates throughout the fatigue process, it can be concluded that the primary direction of the near-surface delamination progression is determined by the fibre direction of the laminate surface ply.

Comparison of the failure mechanisms of the fatigued specimens with those from preliminary

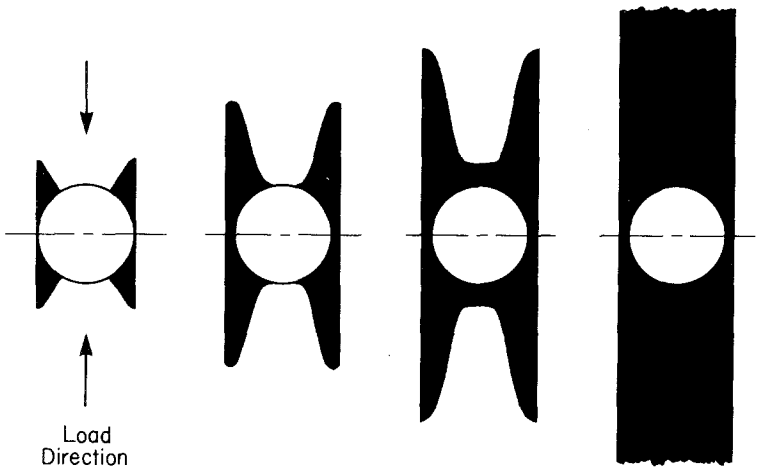

Figure 15 Near-surface delamination growth: Laminate C.

tests on undamaged specimens showed some differences in the fibre-dominated laminates, and no significant difference in the quasi-isotropic laminates. In the case of the fibre-dominated laminates, the indication was that the diagonal shear mode was not dominant in the undamaged specimens, with the net compression mode playing a more significant role than was the case in the fatigued specimens. It should be noted that these results are, as yet, inconclusive due to the small data base involved. However, the implication is that there may be an important link between the fatigue-induced cracking of the laminate and the predominant mode of failure. This is an area which warrants further study.

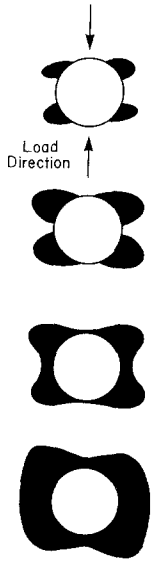

Figure 16 Near-surface delamination growth: Laminate D.

4. Conclusions

The object of this research was the investigation of the effects of compression–compression fatigue on graphite/epoxy laminates containing a 0.635 cm diameter circular hole, with the focus of this paper being on the mechanisms of failure of the laminates subsequent to the fatigue cycling. The results of the tests on the four different laminate configurations revealed the existence of two modes of compressive failure: the diagonal shear (DS) mode and the net compression (NC) mode. The diagonal shear failure was the predominant mode in the fibre-dominant laminates, while the net compression failure was predominant in the quasi-isotropic laminates. The diagonal shear mode was characterized by local instability of small lamina subgroupings which developed as a result of progressive delaminations of the composite. The direction of the laminate shear failure was that of the "sandwiched" angle ply in the lamina subgroupings. The net compression failure was characterized by local instability of individual 0° laminae which were separated due to similar progressive delaminations of the composite.

An important factor related to the modes of failure for the laminates was the nature of the intralaminar cracking which resulted from the fatigue cycling. The laminate stacking sequence played an important role in determining the nature of this cracking. By analysing the stress distribution about the notch, it was found that the positive or negative angle plies were subjected to transverse tension depending on their quadrant location. In Laminates A and B, significant cracking of the angle plies resulted, which is consistent with the predominance of the

diagonal shear failure mode in these laminates. While the nature of the cracking was very similar for these two laminates, there was also a distinction between the two stacking sequences in that the cracking occurred to a lesser degree in Laminate B, and Laminate A also exhibited colinear cracking of the 0° plies tangent to the notch. The quasi-isotropic Laminates C and D, however, did not exhibit any significant intralaminar cracking, which is consistent with the predominance of the net compression failure mode in these laminates. Therefore, the laminate stacking sequence was found to affect the nature of the cracking as well as the mechanism of failure. Preliminary results also indicate the possibility of a direct relation between the nature of the fatigue-induced intralaminar cracking and the predominant failure mode of the laminate.

Throughout the fatigue cycling, non-destructive evaluation (NDE) was carried out by means of ultrasonic C-scan techniques. Based on those results, it was concluded that the primary direction of near-surface delamination is the same as the fibre direction of the laminate surface ply.

An additional factor considered in this study was the effect of the resin system on the failure mechanisms. The results showed no discernable difference between the T300-5208 and T300-5209 resin systems at room temperature.

Acknowledgements

This research was supported by the Materials Science Corporation, Blue Bell, Pa, USA and the US Naval Air Systems Command, Contract No. N00019-79-C-0633.

References

1. M. S. ROSENFELD and S. L. HUANG, Proceedings of the AIAA/ASME 18th Structures, Structural Dynamics and Materials Conference, San Diego, March 1977 (American Institute of Aeronautics and Astronautics, New York, 1977) pp. 423–7.
2. J. M. WHITNEY, I. M. DANIEL and R. B. PIPES, "Experimental Mechanics for Fibrous Composite Materials" Monograph number 4 (Society for Experimental Stress Analysis, Brookfield, Connecticut, 1982).
3. R. B. PIPES, "Experimental Methods for Composite Materials", CCM-79-03 (Center for Composite Materials, University of Delaware, Newark, Delaware, 1979).
4. R. A. BLAKE, Jr, "Ultrasonic NDE of Composite Materials", (Center for Composite Materials, University of Delaware, Newark, Delaware) pp. 1–11.

Received 18 December 1981
and accepted 1 February 1982